IJE TRANSACTIONS B: Applications Vol. 33, No. 8, (August 2020) 1440-1449

International Journal of Engineering

Journal Homepage: www.ije.ir

Numerical Modeling of Non-equilibrium Plasma Discharge of Hydrogenated Silicon Nitride ($SiH_4/NH_3/H_2$)

M. Grari*, C. Zoheir

Mohamed first University, Department of Physics, LETSER Laboratory, Oujda, Morocco

P A P E R I N F O

Paper history:
Received 25 April 2020
Received in revised form 11 June 2020
Accepted 12 June 2020

Keywords:
Numerical Modeling
Non-equilibrium Electron Energy Distribution Function
Radio Frequency Plasma Discharge
Silicon Nitride
Capacitive Coupled Plasma Reactor

A B S T R A C T

In this work, we model a radiofrequency discharge of hydrogenated silicon nitride in a capacitive coupled plasma reactor using Maxwellian and non-Maxwellian electron energy distribution function. The purpose is to investigate whether there is a real advantage and a significant contribution using non-Maxwellian electron energy distribution function rather than Maxwellian one for determining the fundamental characteristics of a radiofrequency plasma discharge. The results show the evolution of the non-Maxwellian electron energy distribution function, the mobility and the diffusion coefficient required to determine the fundamental characteristics of the radiofrequency plasma discharge of a hydrogenated silicon nitride deposit at low pressure and low temperature, between the two electrodes of the capacitive coupled plasma reactor. By comparing these results using non-Maxwellian electron energy distribution function with those calculated using the Maxwellian one, we conclude that the use of non-Maxwellian electronic energy distribution function is more efficient for describing the evolution of a radiofrequency plasma discharge in a capacitive reactor, which will improve the quality of the deposition of thin films.

***doi**: 10.5829/ije.2020.33.08b.01*

NOMENCLATURE

B	Magnetic induction	m_e	Electron mass ($9.11\ 10^{-31}$ kg)
D_e	Electron diffusion coefficient	V_{rf}	Amplitude of the alternative voltages
D_ε	energy transport diffusion	x_k	Molar fraction
E	Electric field	z	Axial cylindrical coordinate
F	Lorentz force	**Greek Symbols**	
f	Equilibrium distribution function	$\mathcal{E}$	Energy
F_0	Non- Equilibrium electronic energy distribution function	ε_0	Vacuum permittivity
K	Number of collision	ϕ	Particle relaxation time
K_B	Boltzmann's constant ($1.381\ 10^{-23}$ J/K)	γ	Acceleration of a particle
K_r	Kinetic coefficient	γ_p	Secondary electron emission coefficient
M	Mass of the species.	λ	Renormalization factor
N	Gas density	μ_e	Electron mobility
N_n	Total density of neutral	μ_{eN}	Energy mobility
n_e	Electron density	π	3.1416
n_i	Ion density	σ_k	effective momentum-transfercross-cross
p	Pressure	σ_m	The total momentum-transfer cross-section
q	Electric charge	Γ	Particle flux

*Corresponding Author Email: *grarimery@gmail.com* (M. Grari)

Please cite this article as: M. Grari, C. Zoheir, Numerical Modeling of Non-equilibrium Plasma Discharge of Hydrogenated Silicon Nitride ($SiH_4/NH_3/H_2$), International Journal of Engineering (IJE), IJE TRANSACTIONS B: Applications Vol. 33, No. 8, (August 2020) 1440-1449

$\boldsymbol{r}$	Spatial vector	$\boldsymbol{\Gamma}_e$	Electron flux
S	Term source	$\boldsymbol{\Gamma}_i$	Ion flux
T	Particles temperature	$\boldsymbol{\Gamma}_\varepsilon$	Energy flux
u	Average velocity	v_{th}	Thermal velocity of electron
v	Velocity vector	$\Delta\varepsilon_k$	Energy loss

1. INTRODUCTION

Hydrogenated silicon nitride has attracted the interest of researchers over the last decades because of its wide application in thin films [1,2]. Hydrogenated amorphous silicon nitride films can be deposited in a capacitive coupled plasma (CCP) reactor because of high electron density and low electron temperature, leading to high-rate depositions of silicon films [3,4]. The plasma discharge in CCP reactor combines several phenomena during deposition: creation of electrical charges by radiofrequency (RF) excitation, fluid flow and chemical reactions on the surface.

The RF plasma discharge is a method that allows obtaining a plasma medium with specific parameters, both geometrically and in terms of the fluid itself. Moreover, it is a method well suited to the description of non-linear phenomena. RF discharges attracted the attention of physicists before their practical applications in the field of physics were known [5-8]. The capacitive RF discharge allows to define a frequency range between 1 and 100 MHz, gas pressure between 1 mTorr and few Torrs with a dimension of about a few cm and a power between 1 and 10 watts. Under these conditions, the RF discharge plasma is weakly ionized and out of thermodynamic equilibrium. The temperature value of the electrons depends in particular on the gas pressure and the discharge conditions.

In order to obtain a high quality of deposition, it is necessary to seek the better characteristics of the plasma discharge in CCP reactor. The fluid model can be used to determine the characteristics of the plasma discharge. The resolution of the fluid model equations is usually done by assuming a Maxwellian electron energy distribution function (EEDF). However, in the sheath regions of the fluid model of a RF discharge, the electron temperature is much higher than the temperature of heavy particles. That is why it is more likely that the real EEDF is non-Maxwellian because of its capability to describe an out-of-equilibrium system with high density and temperature gradients compared to the EEDF Maxwellian one.

Much attention is devoted to the non-equilibrium EEDF, because of their applications in many technological fields [1,9]. Godyac (1990,1995) has shown the existence of two electron groups, characterized by a weak inter-interaction, a significative different temperatures and their energy distribution can be a bi-Maxwellian EEDF [10,11]. Hageleer and Pitchford (2005) [12] developed a new resolution model of the Boltzmann equation (BE) to obtain transport coefficients and diffusion coefficients applicable for fluid models describing much more general conditions.

In this work, we are interested in studying the fundamental characteristics of the capacitive RF plasma discharge of silicon nitride using a non-Maxwellian EEDF which we calculated based on the Boltzmann model developed by Hageleer and Pitchford [12]. Thus, we intend to validate the choice of using the non-Maxwellian EEDF. Then, we focus on comparing the plasma discharge characteristics obtained using the non-Maxwellian EEDF with those calculated by a Maxwellian distribution function.

This article is organized as follows. In Section 2, we briefly describe the hypothesis and mathematical formulations used for determining non-equilibrium EEDF and transport coefficients. In Section 3, we describe hybrid physical model of plasma discharge using a non equilibrium EEDF. In Section 4, we present and compare the simulation results obtained by using a non-Maxwellian and Maxwellian EEDF. Finally, the conclusion is set out in Section 5.

2. CALCULATION OF EEDF, MOBILITY AND DIFFUSION COEFFICIENTS

2. 1. EEDF Calculation In general, the transport of charged species in the plasma can be described by the Boltzmann equation:

$$\frac{\partial f}{\partial t} + \mathbf{v}\nabla_r f + \frac{\mathbf{F}}{m_e}\nabla_v f = C[f] \quad (1)$$

which is a continuity equation in phase space (***r***, **v**). The right side of equation (1) is the collision operator, which describes the interaction between the particles in the system.

In our adopted model, we have three approximations:

- The initiating electric field and the probability of collision are uniform.
- The distribution of the electrons is then symmetrical around the direction of the electric field.
- In position, the electron distribution space can only change in the direction of the applied electric field.

Using the spherical coordinates in velocity space and choosing the direction *z* we obtain:

$$\frac{\partial f}{\partial t}+v\cos\theta\frac{\partial f}{\partial z}+\frac{e}{m_e}E\left(\cos\theta\frac{\partial f}{\partial v}+\frac{sin^2\theta}{v}\frac{\partial f}{\partial\cos\theta}\right)=C[f] \quad (2)$$

Such as $v=\left(v_x{}^2+v_y{}^2+v_z{}^2\right)^{1/2}$

The function f in Equation (2) depends on four variables: z, v, θ and t. Using the two-term approximation [12-14] we can simplify the dependence of the function f on θ to obtain Equation (3):

$$f(z,v,\theta,t)=f_0(z,v,t)+\cos\theta f_1(z,v,t) \quad (3)$$

The function f is the sum of a part isotrope f_0 and a small anisotropic perturbation f_1 [12,15].

According to the work [13,15] we can separate the energy dependence of f from its dependence on time and space by assuming that :

$$f(\varepsilon,z,t)=\frac{1}{2\pi\gamma^3}F_0(\varepsilon)n(z,t) \quad (4)$$

with F_0 is the energy distribution function which is constant in time and space, and $\gamma=\left(\frac{2e}{m_e}\right)^{1/2}$.

A further simplification on f in Equation (4) can be made with respect to time. Indeed, the electric field and the distribution of electrons can be considered to be stationary or oscillating at high frequency.

Based on the previous simplifications and the collision term calculation, Hageleer and Pitchford [12] have shown Equation (5).

The term to the left of Equation (5) represents a convection part with negative flow velocity $\tilde{W}$ and a diffusion part with coefficient $\tilde{D}$.

$$\frac{\partial}{\partial\varepsilon}\left(\tilde{W}F_0-\tilde{D}\frac{\partial F_0}{\partial\varepsilon}\right)=\tilde{S}$$

$$\tilde{W}=-\gamma\varepsilon^2\sigma_\varepsilon-3a\frac{n}{N}A_1$$

$$\tilde{D}=\frac{\gamma}{3}\left(\frac{E}{N}\right)^2\frac{\varepsilon}{\tilde{\sigma}_m}+\frac{\gamma k_BT}{e}\varepsilon^2\sigma_\varepsilon+2a\frac{n}{N}\left(A_2+\varepsilon^{3/2}A_3\right)$$

where:

$$a=\frac{q^2\gamma}{24\pi\varepsilon_0{}^2}ln\Lambda \quad ; \quad \Lambda=\frac{12\pi\left(\varepsilon_0k_BT_e\right)^{3/2}}{e^3n^{1/2}} \quad (5)$$

$$\sigma_m=\sum_{k=all}x_k\sigma_k \quad ;\sigma_\varepsilon=\sum_{k=elastic}2\left(\frac{m_e}{M}\right)x_k\sigma_k$$

$$\tilde{\sigma}_m=\sigma_m+\frac{\lambda}{\varepsilon^{1/2}} \quad ; \tilde{\sigma}_m=\sigma_m+\frac{\lambda}{\varepsilon^{1/2}};$$

$$A_1=\int_0^\varepsilon u^{\frac{1}{2}}f(u)du; \quad A_2=\int_0^\varepsilon u^{\frac{3}{2}}f(u)du$$

$$A_3=\int_0^\infty f(u)du$$

The source term $\tilde{S}$ represents the energy loss due to inelastic collisions. It can be broken down into three parts: attachment, excitation and ionization.

$$\tilde{S}=\sum_{k=inelastic}C_{0,k}+G$$

$$C_{0,k_{exitation}}=-\gamma x_k\left[\varepsilon\sigma_k(\varepsilon)f(\varepsilon)-(\varepsilon+\Delta\varepsilon_k)\sigma_k(\varepsilon+\Delta\varepsilon_k)f(\varepsilon+\Delta\varepsilon_k)\right]$$

$$C_{0,k_{attachment}}=-\gamma x_k\varepsilon\sigma_k(\varepsilon)f(\varepsilon) \quad (6)$$

$$C_{0,k_{ionization}}=-\gamma x_k\left[\varepsilon\sigma_k(\varepsilon)f(\varepsilon)-(\varepsilon+\Delta\varepsilon_k)\sigma_k(\varepsilon+\Delta\varepsilon_k)f(\varepsilon+\Delta\varepsilon_k)\right]+\delta\gamma x_k\varepsilon\sigma_k(\varepsilon)f(\varepsilon)$$

$$G=-\gamma\lambda f\varepsilon^{1/2}$$

The term λ is a scalar renormalization factor, which ensures that the EEDF has the following property:

$$\int_0^\infty f\varepsilon^{1/2}d\varepsilon=1$$

The left side of Equation (3) is discretized by the exponential scheme [15].

2. 2. Mobility and Electrons Diffusion The knowledge of the distribution function has allowed us to determine a number of important parameters, such as the ionization rate by collision of electrons, the mobility of electrons, the diffusion rate, the average energy of electrons, etc.

For the electrons transport, the mobility and diffusion of electrons are given by Equations (7) and (8):

$$\mu_e=-\frac{\gamma}{3}\int_0^\infty\frac{\varepsilon}{\hat{\sigma}}\frac{\partial F_0}{\partial\varepsilon}d\varepsilon \quad (7)$$

$$D_e=\frac{\gamma}{3}\int_0^\infty\frac{\varepsilon}{\hat{\sigma}}F_0d\varepsilon \quad (8)$$

For the energy transport, the mobility and diffusion of electrons are given by Equations (9) and (10):

$$\mu_\varepsilon=-\frac{\gamma}{3\bar{\varepsilon}}\int_0^\infty\frac{\varepsilon^2}{\hat{\sigma}}\frac{\partial F_0}{\partial\varepsilon}d\varepsilon \quad (9)$$

$$D_\varepsilon=\frac{\gamma}{3}\int_0^\infty\frac{\varepsilon^2}{\hat{\sigma}}F_0d\varepsilon \quad (10)$$

3. Hybrid Physical Model Like other reactors used in industry [16-21], the CCP reactor involves a set of fairly complex physico-chemical processes. The physical model must describe the dynamics of the plasma medium. In addition, it must take into account chemical reactions that best describe the source terms. We used a macroscopic-microscopic hybrid model where the fluid equations describe the kinetics of the system and the source terms are computed from the non-equilibrium EEDF.

The plasma dynamics is described by taking into account excitation phenomena, radical, ion dissociation, and their collisions with electrons. Efficient cross-sections were considered over a wide range of energy. This allows us to better describe the chemical reactions in volume of the species generated by the dissociation and recombination of neutral and radical particles, as well as the surface reactions on the substrate. The fluid flow rate describes the transfer of heat and mass into the reactor. All these phenomena are modeled by a system of equations, non-linear and dispersive, described in the following sections. The differential equations are solved using the finite element method.

To summerize the research methodology adapted in this article, we present this flowchart in Figure 1.

3. 1. CCP Reactor Figure 2 shows a synoptic scheme of a symmetrical CCP reactor which is composed of two parallel conductive electrodes, a gas pump and a substrate. The working gases are introduced at the inlet, and then brought into the reaction chamber,

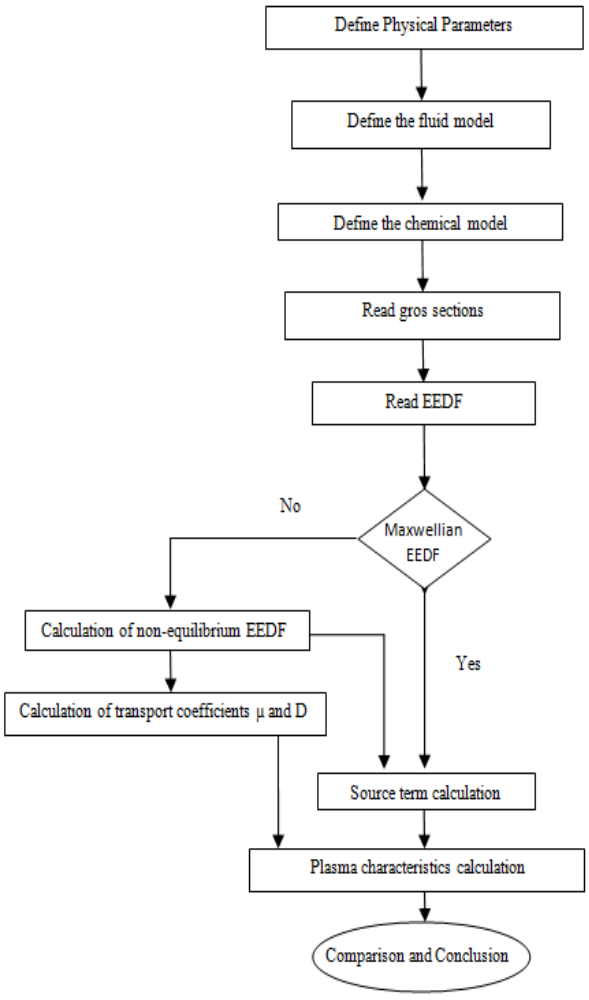

Figure 1. Flowchart of the proposed research methodology

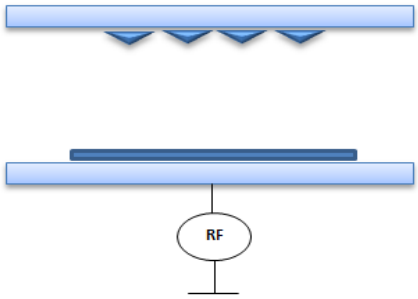

Figure 2. Synoptic scheme of CCP reactor used for plasma deposition of thin films

where a series of volume and surface reactions take place resulting in a deposition of thin films on the substrate.

The plasma in the CCP reactor are at low pressure, low electronic temperature and low ionization rate. In a mixture of ammonia and hydrogen silicon, the gas pressure between 0.2 and 0.5 Torr, the frequency is about 13.56 MHz, the voltage is 130 V, and the space between electrodes varies between 2.7 and 6 cm.

3. 2. Equations The general equations for a plasma discharge [15, 22] are calculated taking into account the following hypotheses:

-The gas is weakly ionized.
-The pressure is low.
-No magnetic field is applied.
-The electrons are supposed to have a non-Maxwellian energy distribution function.
-The mobility and the diffusion coefficients are calculated by the non-Maxwellian EEDF.

In our model we solve the system of equations (11)-(16) corresponding to a set of low temperature plasma evolution equations related to the self-coherent field $\boldsymbol{E}$ by Poisson's equation (17).

-Electron and ion transport

$$\frac{\partial n_e}{\partial t} + \nabla \boldsymbol{\Gamma}_e = S_e \tag{11}$$

$$\frac{\partial n_i}{\partial t} + \nabla \boldsymbol{\Gamma}_i = S_i \tag{12}$$

-Electron and ion flux

$$\boldsymbol{\Gamma}_e = -n_e \mu_e \boldsymbol{E} - \nabla(n_e D_e) \tag{13}$$

$$\boldsymbol{\Gamma}_i = -n_i \mu_i \boldsymbol{E} - \nabla(n_i D_i) \tag{14}$$

-Electron energy

$$\frac{\partial n_\varepsilon}{\partial t} + \nabla \boldsymbol{\Gamma}_\varepsilon + \boldsymbol{E}\boldsymbol{\Gamma}_e = S_\varepsilon \tag{15}$$

-Energy flux

$$\Gamma_\varepsilon = -n_\varepsilon \mu_\varepsilon E - \nabla(n_\varepsilon D_\varepsilon) \quad (16)$$

-Electric field

$$\varepsilon_0 \nabla E = e(n_e - n_i) \quad (17)$$

-Source terms

$$S_e = \sum x_r k_r N_n n_e \quad (18)$$

$$S_i = \sum x_r k_r N_n n_i \quad (19)$$

$$S_\varepsilon = \sum x_r k_r N_n n_e \varepsilon_r \quad (20)$$

$$k_r = \sqrt{2e/m_e} \int \varepsilon \sigma_r(v) F_0(\varepsilon) d\varepsilon \quad (21)$$

F_0 is the non-Maxwellian EEDF.

3. 3. Chemical Reactions The calculation of the source term equations (18)-(21), in the fluid model is based on the distribution function calculated by the model of Boltzmann F0 plus gross sections $\sigma_r(v)$ which takes into account the most reactive elastic and inelastic excitation and ionization collisions, presented in Table 1.

The cross sections data used in simulation, SiH_4 and NH_3 collisions are given by Hayashi [23].

The chemical species considered in this work are presented in Table 2. These species are very important for plasma chemistry and have an influence on the deposition process.

3. 4. Boundary Conditions The boundary conditions used in this section are similar to those presented by Bavafa et al. [2] and Xia et al. [24].

-The boundary condition for Poisson's equation is the potential value on the electrodes:

$V = 0$ electrical potential at the cathode.

TABLE 1. Energy of reactions NH3 SiH4

Reactions	Energy (eV)
1 : e+NH_3 => e+NH_3^*	0.202
2 : e+NH_3 => e+NH_3^*	0.42
3 : e+NH_3 => e+NH_3^*	5.72
4 : e+NH_3 => e+NH_3^*	8.65
5 : e+NH_3 => 2e+NH_3^+	10.2
6 : e+SiH_4 => e+SiH_4^*	0.115
7 : e+SiH_4 => e+SiH_4^*	0.27
8 : e+SiH_4 => e+SiH_4^*	8.01
9 : e+SiH_4 => e+SiH_4^*	8.92
10 : e+SiH_4 => 2e+SiH_4^+	12.9

TABLE 2. Kinetic coefficient of reactions NH_3 SiH_4

Reactions	Kinetic Coefficient $m^3/(s.mol)$
7 : SiH_4 + SiH_2 => Si_2H_6	2.8 10^7
8 : SiH_4 + H => SiH_3 + H_2	1.9 10^6
9 : SiH_4 + NH => $HSiNH_2$ + H_2	3.6 10^6
10 : SiH_4 + NH_2 => SiH_3 + NH_3	2.4 10^6
11 : SiH_4 + NH => SiH_3 + NH_2	2.4 10^7

$V_{rf} = V_0 \sin(\omega t)$ electrical potential at the anode.

- The boundary condition for electrons has a flow proportional to their thermal velocity, while for ions it has a zero gradient near the walls:

$$\Gamma_e = 5\frac{v_{th} n_e}{4} - \gamma \Gamma_i$$

$$\Gamma_i = -\mu_i n_i \nabla V$$

-Quantities v_{th} and q_e are calculated by:

$$q_e = \frac{v_{th} k_B}{4} \qquad v_{th} = \sqrt{\frac{8 k_B T_e}{\pi m_e}}$$

4. RESULTS AND DISCUSSION

To investigate the plasma discharge characteristics in the CCP reactor, the fluid approach are considered. Using the Boltzmann equation [12] we calculate the non-Maxwellian EEDF, the mobility and diffusion coefficients. Based on these factors we proceed to the resolution of the fluid model equations. Thus, we obtain the plasma discharge characteristics that will be used in the start to validate the choice of the non-Maxwellian EEDF, then to compare them with the plasma discharge characteristics obtained using Maxwellian EEDF.

In our simulations, the CCP reactor is driven by a sinusoidal voltage with a frequency of 13.56 MHz at a temperature of 573 K. Silicon diluted with hydrogen and ammoniac mixture is used as a deposition precursor gas. The RF voltage taken has an amplitude of 130 V, applied to the anode for an inter-electrode distance d and a variable pressure p. The results are presented at a final relaxation calculation time of around 7.37 μs.

Figure 3 shows the evolution of non-Maxwellian EEDF for $SiH_4/NH_3/H_2$ gases in energy range between 3 and 10 eV. The non-Maxwellian EEDF is calculated from the reactions presented in Table 1, the initial energy is $\varepsilon = 3\text{eV}$. This non-Maxwellian EEDF will be used in the source terms of the fluid model to calculate the density and the energy electrons.

The mobilities equations (7) and (9) and diffusion coefficients equations (8) and (10), calculated by the non-Maxwellian EEDF, are shown in Figure 4. They

will be used to calculate electron ion and energy flux in Equations (13), (14) and (16).

For the validation of the non-Maxwellian EEDF, we will discuss Figures 4-9. Therefore, Figures 5-7 show the variation of electron density, temperature and electric field as a function of pressure, taking a pressure margin between 0.2 and 0.5 Torr for an inter-electrode distance of 2.7 cm. Keeping the pressure at 0.3 Torr and varying the distance between 3 and 6 cm, Figures 8-10 show respectively the variation of the electron density, the temperature and the electric field as a function of the distance. Finally, Figures 11-13 show the comparison of density, temperature and electric field calculated by a Maxwellian and non-Maxwellian EEDF.

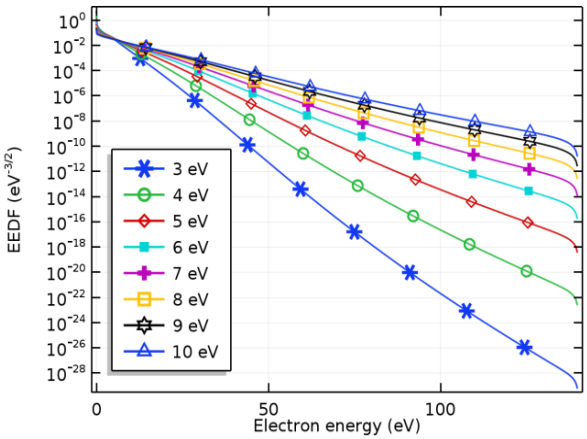

Figure 3. The evolution of Boltzmann's EEDF of SiH_4 NH_3 plasma in an energy range between 3 and 10 eV

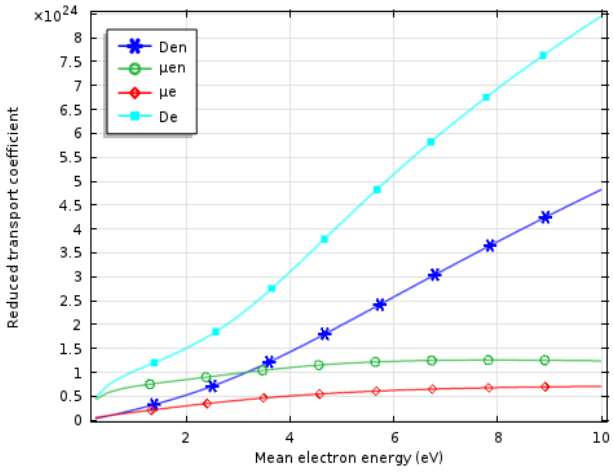

Figure 4. Reduced transport coefficients calculated by the non-Maxwellian EEDF

where, De: Reduced electron energy diffusivity (1/(m*s)), Den: Reduced electron diffusivity (1/(m*s)), μen: Reduced electron energy mobility (s^2 *A/(m^3*kg)), μe: Reduced electron mobility (s^2 *A/(m^3*kg))

By increasing the pressure in the deposition system, the density of radicals grows as the density of precursors increases (Figure 5). Another effect of the increase in the pressure of the deposition chamber is the fact that it leads to the accumulation of radicals in the area between ducts, which reduces the temperature in this area (Figure 6).

An electric field is introduced and added to the field created by the charges in the plasma. Figure 7 shows that it becomes important when the pressure increases, causing a significant displacement of electrons and ions. The field perceived by the electrons is very strong and allows the electrons to accelerate towards the anode. The migration of electrons from the cathode to the anode produces a higher temperature at the anode and therefore the temperature attenuation at the cathode, which is verified in Figure 6. These results are consistent with Daoxin et al. [25].

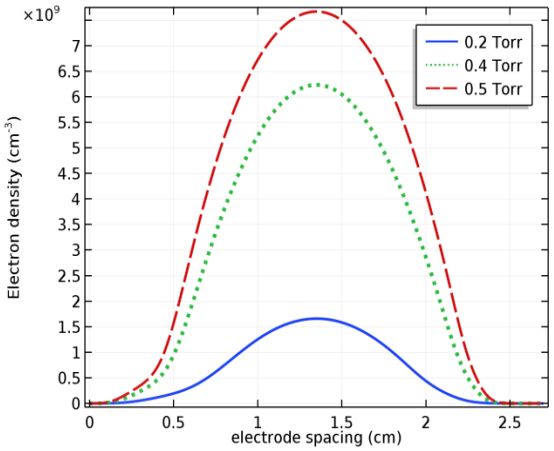

Figure 5. Variation of the electronic density as a function of pressure using non-Maxwellian EEDF

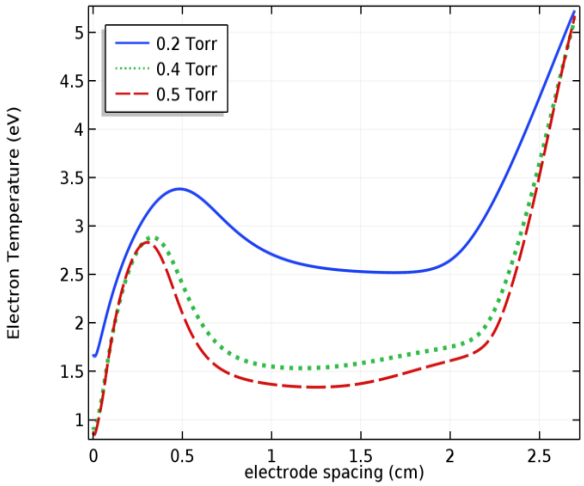

Figure 6. Variation of the electronic temperature as a function of pressure using non-Maxwellian EEDF

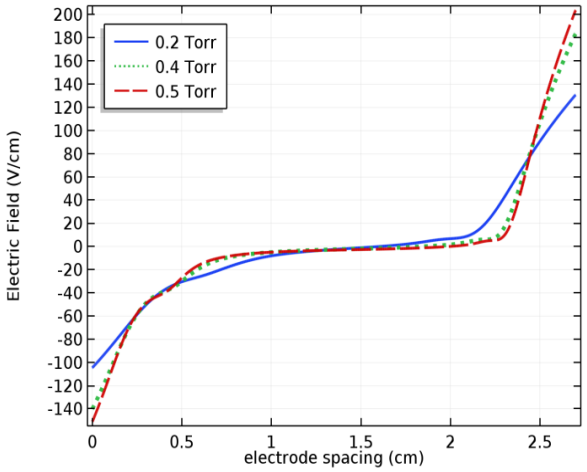

Figure 7. Variation of the electric field as a function of pressure using non-Maxwellian EEDF

The influence of the inter-electrode distance on the discharge is shown in Figures 8-10. When the distance becomes larger, collisions between electrons decrease and therefore the creation of secondary electrons will be low. In addition, as the distance increases, there is an expansion of the density towards the electrodes. These results are the same to that of Bavefa et al. [2] and Samir et al. [26] with respect to electron density, electron temperature and electric field distributions.

Summing up, according to these results and based on the comparison with theoretical [15, 22] and practical literature works [2, 9, 27-29], we validate the choice of the non-Maxwellian distribution function. Indeed, the plasma caracteristics resulting from the use of the non-Maxwellian EEDF satisfy the normal evolution of RF plasma discharge.

For an inter-electrode distance of 5 cm, and a pressure of 0.3 Torr, Figures 11-13 show respectively the variation in electron density, temperature and electric field, determined using the Maxwellian and non-Maxwellian EEDF.

Figure 11 shows that the density calculated based on a non-Maxwellian EEDF is much higher than that calculated using a Maxwellian EEDF. Indeed, the non-Maxwellian EEDF provides an electron density of about 3.9 $x10^9$ cm^{-3} while the Maxwellian EEDF barley reaches 2.5 $x10^9$ cm^{-3}. This significant difference in electron density means that there is another type of faster electrons added which couldn't be shown by using Maxwellian EEDF, while the use of the non-Maxwellian EEDF has succeed to reveal it. Figure 12 shows that the electron temperature calculated using a non-Maxwellian EEDF (about 13 eV) is higher than the calculated one using a Maxwellian EEDF (about 9 eV). This result is due to the high speed of electrons (about 3.4 $x10^8$cm/s) obtained using non-Maxwellian EEDF compared to that using Maxwellian EEDF (about 2.5x 10^8 cm/s) shown in Figure 13. These electrons have a self-coherent field source, hence the increase in the amplitude of the electric field at the cathode (Figure 14).

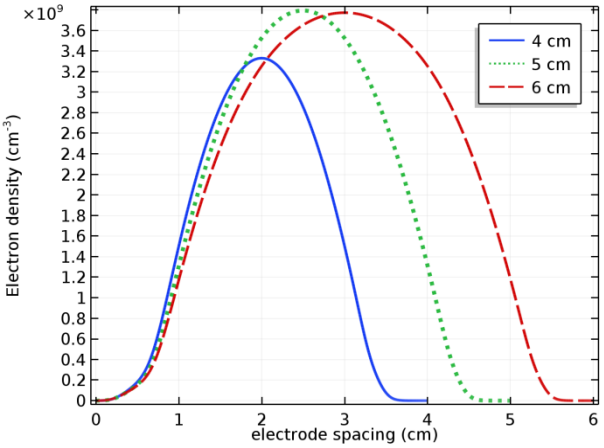

Figure 8. Variation of the electronic density as a function of distance using non-Maxwellian EEDF

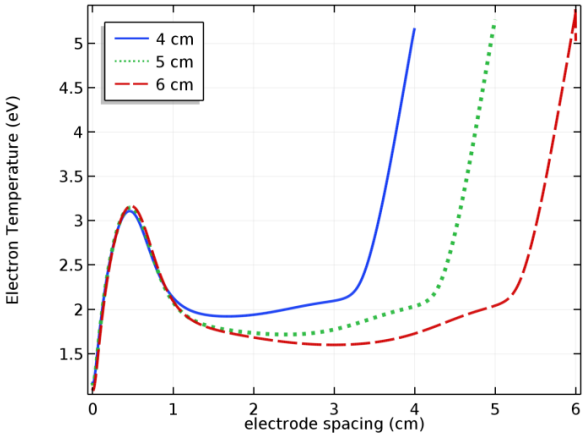

Figure 9. Variation of the electronic temperature as a function of distance using non-Maxwellian EEDF

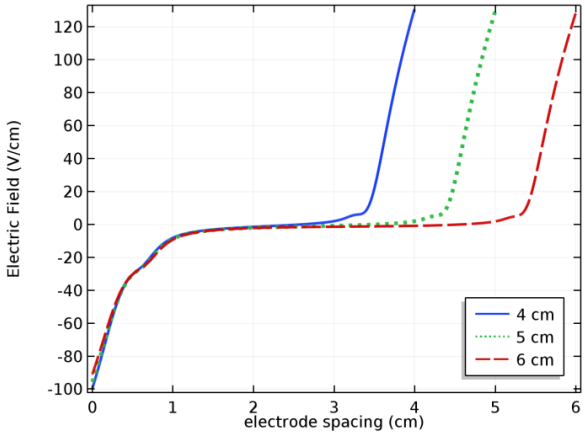

Figure 10. variation of the electric field as a function of distance using non-Maxwellian EEDF

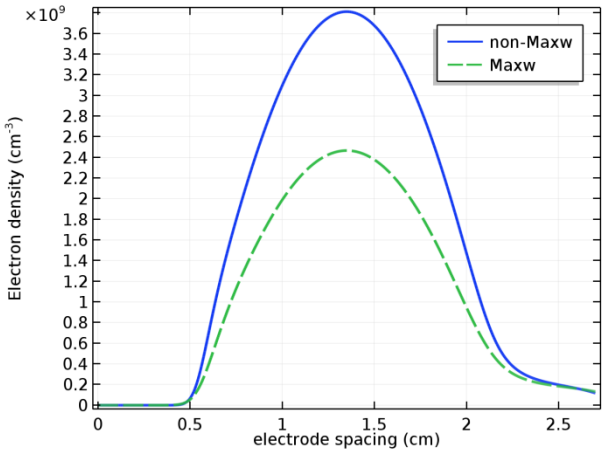

Figure 11. Electron density comparison using Maxwellian and non-Maxwellian EEDF

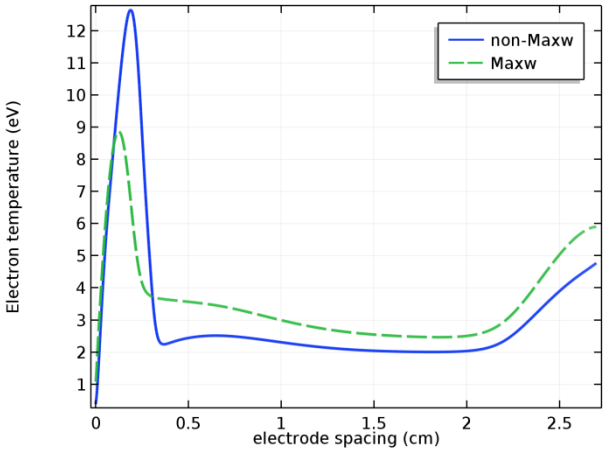

Figure 12. Electron temperature comparison using Maxwellian and non-Maxwellian EEDF

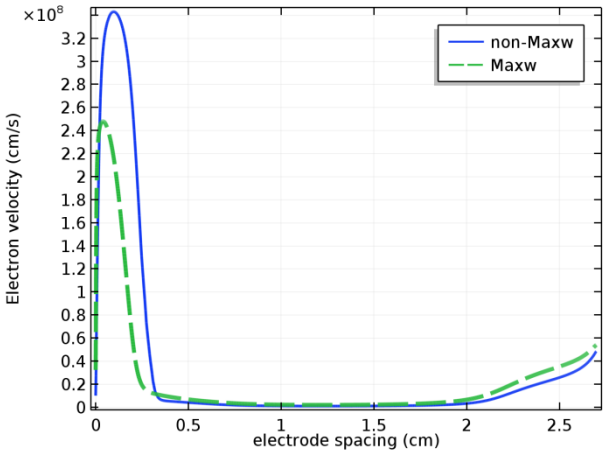

Figure 13. Electron velocity comparison using Maxwellian and non-Maxwellian EEDF

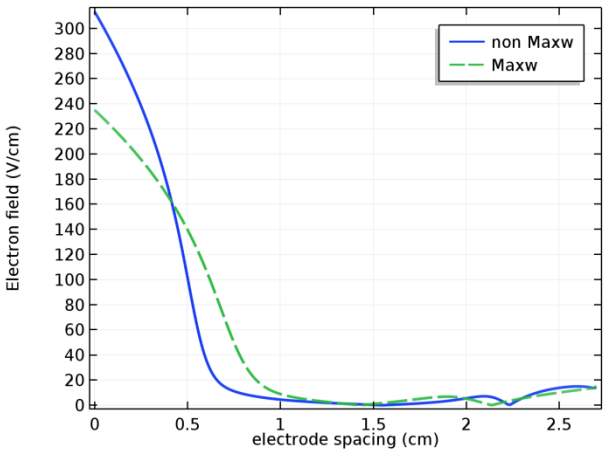

Figure 14. Electric field comparison using Maxwellian and non-Maxwellian EEDF

The field allows electrons to accelerate towards the anode. This migration produces a higher temperature at the anode, and hence temperature attenuation at the cathode (Figure 12).

5. CONCLUSION

In this work, we used a one-dimensional fluid model based on a non-Maxwellian electron energy distribution function to describe the characteristics of capacitive coupled plasma excited by an RF source using silane diluted with ammoniac and hydrogen ($SiH_4/NH_3/H_2$). The discharge operates at 13.56 MHz with RF voltage amplitude of 130 V and simulated at variable pressures and inter-electrode distances. The aim was to validate the choice of the non-Maxwellian EEDF and to compare the evolution of the plasma discharge characteristics obtained using the non-Maxwellian EEDF with those calculated by using a Maxwellian one.

By varying the pressure and distance between electrodes, we validated the choice of the non-Maxwellian EEDF and the type of the used gas. Indeed, the results show a significant increase in density when the gas pressure grows in the range of 0.2 to 0.5 Torr, similarly, when the inter-electrode distance increases in the range of 4 to 6 cm.

The use of a non-Maxwellian EEDF allowed us to reveal the existence of another faster type of electrons, which was not detected when a Maxwellian EEDF was used. Indeed, in the non-Maxwellian case an average electron velocity of about 3.4 $x10^8$ cm/s and an electron temperature of 13 eV were obtained at the cathode, whereas in the Maxwellian case an average electron velocity of about 2.4 $x10^8$ cm/s and an electron temperature of 9 eV were barely reached at the cathode. In addition, compared with the Maxwellian EEDF the

plasma discharge obtained using the non-Maxwellian EEDF has a higher electron density of about 3.8 $x10^{9}cm^{-3}$ which increases the deposition rate, and a reduced temperature at the anode of about 4.8 eV which results in a better distribution of species at the surface.

We deduce that the non-Maxwellian approximation of the electron energy distribution function is more effective to describe the evolution of an RF plasma discharge in a capacitive reactor than the Maxwellian one. Thus, in order to ensure better deposition of thin films, it is recommended to define the electron transport properties by an electron energy distribution function using a non-Maxwillian EEDF, which is a closer assumption to the real conditions of the physical model. Consequently, the application of this function in our fluid model for the discussion of gas type selection, pressure and inter-electrode distance, will provide better characteristics to enhance the quality of CCP reactor.

Finally, it will be interesting in a future work to seek optimal deposition of thin films by studying a two-dimensional simulation using a non-Maxwellian EEDF.

6. REFERENCES

1. Su, L. W., Chen, W., Uchino, K., and Kawai, Y., "Two-dimensional simulations of multi-hollow VHF SiH4/H2 plasma", ***AIP Advances***, Vol. 8, No. 2, (2018), 025316. DOI: 10.1063/1.5003911.
2. Bavafa, M., Ilati, H., Rashidian, B., "Comprehensive simulation of the effects of process conditions on plasma enhanced chemical vapor deposition of silicon nitride", ***Semiconductor Science and Technology***, Vol. 23, No. 9, (2008), 095023. DOI: 10.1088/0268-1242/23/9/095023.
3. Kim, H. J., Wonkyun Y., and Junghoon J., "Effect of electrode spacing on the density distributions of electrons, ions, and metastable and radical molecules in SiH4/NH3/N2/He capacitively coupled plasmas", ***Journal of Applied Physics***, Vol. 118, No. 4, (2015), 043304. DOI: 10.1063/1.4927531.
4. Kim, H. J., and Hae June L., "2D fluid model analysis for the effect of 3D gas flow on a capacitively coupled plasma deposition reactor", ***Plasma Sources Science and Technology***, Vol. 25, No. 3, (2016), 035006. DOI: 10.1088/0963-0252/25/3/035006
5. Graves, D. B., and Jensen, K. F, "A continuum model of DC and RF discharges", ***IEEE Transactions on Plasma Science***, Vol. 14, No. 2, (1986), 78-91. DOI: 10.1109/TPS.1986.4316510.
6. Passchier, J. D. P., and Goedheer, W. J., "A twodimensional fluid model for an argon rf discharge", ***Journal of Applied Physics***, Vol. 74, No. 6, (1993), 3744-3751. DOI: 10.1063/1.354487.
7. Li, X. S., Bi, Z. H., Chang, D. L., Li, Z. Wang,C., S., Xu, X., Xu, Y., Lu, W. Q., Zhu, A. M., and Wang, Y. N., "Modulating effects of the low-frequency source on ion energy distributions in a dual frequency capacitively coupled plasma", ***Applied Physics Letters***, Vol. 93, (2008), No. 3, 031504. DOI: 10.1063/1.2945890.
8. Grari, M., and Zoheir, C., "Numerical Modeling of Plasma Silicon Discharge for Photovoltaic Application", ***Materials Today: Proceedings***, Vol. 13, (2019), 882-888. DOI: 10.1016/j.matpr.2019.04.052.
9. Wang, X. F., Jia, W. Z., Song, Y. H., Zhang, Y. Y., Dai, Z. L., and Wang, Y. N., "Hybrid simulation of electron energy distributions and plasma characteristics in pulsed RF CCP sustained in Ar and SiH4/Ardischarges", ***Physics of Plasmas***, Vol. 24, No. 11, (2017), 113503. DOI: 10.1063/1.5009416.
10. Godyak, V. A., and Piejak, R. B., "Abnormally low electron energy and heating-mode transition in a low-pressure argon rf discharge at 13.56 MHz", ***Physical Review Letters***, Vol. 65, No. 8, (1990), 996. DOI: 10.1063/1.5009416.
11. Godyak, V. A., Meytlis, V. P., and Strauss, H. R., "Tonks-Langmuir problem for a bi-Maxwellian plasma", ***IEEE Transactions on Plasma Science***, Vol. 23, No. 4, (1995), 728-734. DOI: 10.1109/27.467995.
12. Hagelaar,G. J. M., and Pitchford, L. C., "Solving the Boltzmann equation to obtain electron transport coefficients and rate coefficients for fluid models", ***Plasma Sources Science and Technology***, Vol. 14, No. 4, (2005), 722. DOI: 10.1088/0963-0252/14/4/011.
13. Pitchford, L. C., and Phelps, A. V., "Comparative calculations of electron-swarm properties in N2 at moderate E/N values", ***Physical Review A***, Vol. 25, No. 1, (1982), 540. DOI: 10.1103/PhysRevA.25.540.
14. Godyak, V. A., "Nonequilibrium EEDF in gas discharge plasmas", ***IEEE Transactions on Plasma Science***, Vol. 34, No. 3, (2006), 755–766. DOI: 10.1109/TPS.2006.875847.
15. Lieberman, M. A., and Lichtenberg, A. J., "Principles of plasma discharges and materials processing", John Wiley & Sons, 2005.
16. Abdelaal, A. M., Attalla, E. M., and Elshemey, W. M., "Estimation of Out-of-Field Dose Variation using Markus Ionization Chamber Detector", ***SciMedicine Journal***, Vol. 2, No. 1, (2020), 8-15. DOI: 10.28991/SciMedJ-2020-0201-2
17. Sanito, R. C., You, S. J., Chang, G. M., and Wang, Y. F., "Effect of shell powder on removal of metals and volatile organic compounds (VOCs) from resin in an atmospheric-pressure microwave plasma reactor", ***Journal of Hazardous Materials***, (2020), 122558. DOI: 10.1016/j.jhazmat.2020.122558.
18. Ali, A., Ejaz, N., Nasreen, S., Nasir, A., Qureshi, L. A., and Al-Sakkaf, B. M. "Enhanced Degradation of Dyes present in Textile Effluent by Ultrasound Assisted Electrochemical Reactor", ***Civil Engineering Journal***, Vol. 5, No. 10, (2019), 2131-2142. DOI: 10.28991/cej-2019-03091399.
19. Shoukat, R., and Khan, M. I., "Synthesis of nanostructured based carbon nanowalls at low temperature using inductively coupled plasma chemical vapor deposition (ICP-CVD)". ***Microsystem Technologies***, Vol. 25, No. 12, (2019), 4439-4444. DOI: 10.1007/s00542-019-04463-7.
20. Archin, S., "Optimization of Process Parameters by Response Surface Methodology for Methylene Blue Removal Using Cellulose Dusts", ***Civil Engineering Journal***, Vol. 4, No. 3, (2018). DOI: 10.22090/JWENT.2018.02.007.
21. Ghorbani, H., Poladi, A., and Hajian, M., "Pulsed DC-Plasma Assisted Chemical Vapor Deposition of α-rich Nanostructured Tantalum Film: Synthesis and Characterization", ***International Journal of Engineering***, ***Transactions A: Basics,*** Vol. 30, No. 4 , (2017), 551-557. DOI: 10.5829/idosi.ije.2017.30.04a.13.
22. Capitelli, M. R., Celiberto, Colonna, G., Esposito, F., Gorse, C., Hassouni, K., Laricchiuta, A., and Longo, S., "Fundamental aspects of plasma chemical physics: kinetics", Springer Science and Business Media, 2015.
23. Hayashi database, www.lxcat.net, retrieved on October 27, 2016.
24. Xia, H., Xiang, D., Yang, W., Mou, P., "Multi-model simulation of 300mm silicon-nitride thin-film deposition by PECVD and experimental verification", ***Surface and Coatings Technology***, Vol. 297, (2016), 1-10. DOI: 10.1016/j.surfcoat.2016.04.034.

25. Daoxin, H., Jia, C., Linhong, J. and Yuchun, S., "Simulation of cold plasma in a chamber under high-and low-frequency voltage conditions for a capacitively coupled plasma", ***Journal of Semiconductors***, Vol. 33, No. 10, (2012), 104004. DOI: 10.1088/1674-4926/33/10/104004.

26. Samir, T., Liu, Y., Zhao, L.L. and Zhou, Y.W., "Effect of driving frequency on electron heating in capacitively coupled RF argon glow discharges at low pressure", ***Chinese Physics B***, Vol. 26, No. 11, (2017), 115201. DOI: 10.1088/1674-1056/26/11/115201.

27. Ghorbani, H., and Poladi, A., "MD-Simulation of Duty Cycle and TaN Interlayer Effects on the Surface Properties of Ta Coatings Deposited by Pulsed-DC Plasma Assisted Chemical Vapor Deposition", ***International Journal of Engineering, Transactions B: Applications*** Vol. 33, No. 5, (2020), 861-869. DOI: 10.5829/ije.2020.33.05b.18.

28. Kim, H. J., and Lee, H. J. "Analysis of intermediate pressure SiH4/He capacitively coupled plasma for deposition of an amorphous hydrogenated silicon film in consideration of thermal diffusion effects", ***Plasma Sources Science and Technology***, Vol. 26, No. 8, (2017), 085003. DOI: 10.1088/1361-6595/aa78b4.

29. Rastani, S., "Process Optimization of Deposition Conditions for Low Temperature Thin Film Insulators used in Thin Film Transistors Displays", ***International Journal of Engineering, Transactions B: Applications,*** Vol. 31, No. 5, (2018), 712-718. DOI: 10.5829/ije.2018.31.05b.05.

Persian Abstract

چکیده

در این پژوهش، یک تخلیه‌ی بسامد رادیویی از نیترید سیلیکون هیدروژنه در یک راکتور پلاسمای خازنی با استفاده از توابع توزیع انرژی الکترونی ماکسولی و غیرماکسولی مدل‌سازی شده است. هدف بررسی این مطلب است که آیا با استفاده از عملکرد توزیع انرژی غیرماکسولی به جای ماکسولی برای تعیین خصوصیات اساسی تخلیه پلاسمای بسامد رادیویی یک مزیت واقعی و کمک چشم‌گیری حاصل می‌شود یا نه. نتایج تکامل تابع توزیع انرژی الکترونیکی غیرماکسولی تحرک و ضریب انتشار مورد نیاز برای تعیین ویژگی‌های اساسی تخلیه پلاسمای بسامد رادیویی یک رسوب نیترید سیلیکونی هیدروژنه در فشار کم و دمای پایین بین دو الکترود راکتور پلاسمای خازنی را نشان می‌دهد. از مقایسه نتایج به دست آمده با استفاده از تابع توزیع انرژی الکترونیکی غیرماکسولی با نتایج محاسبه شده از طریق ماکسولی نتیجه می‌گیریم که استفاده از عملکرد توزیع انرژی الکترونیکی غیرماکسولی برای توصیف تکامل تخلیه پلاسمای بسامد رادیویی در یک راکتور خازنی کارآمدتر است، که باعث افزایش کیفیت رسوب فیلم های نازک می‌شود.